REPORT

Mimicking *Mytilus edulis* foot protein: A versatile strategy for robust biomedical coatings

Zeyu Du,[1,2] Feng Qiao,[1] Liping Tong,[3] Wentai Zhang,[2] Xiaohui Mou,[1,2] Xin Zhao,[4] Manfred F. Maitz,[1,5] Huaiyu Wang,[3,6,*] Nan Huang,[2,7] and Zhilu Yang[1,2,*]
*Correspondence: hy.wang1@siat.ac.cn (H.W.); zhiluyang1029@swjtu.edu.cn (Z.Y.)
Received: March 27, 2024; Accepted: June 28, 2024; Published Online: June 29, 2024; https://doi.org/10.1016/j.xinn.2024.100671

PUBLIC SUMMARY

- Catechol-decorated polyallylamines (CPA) mimic Mefp-5 for surface engineering.
- "Reinforced concrete-like" structure endows coatings with mechanochemical robustness.
- The abundant grafting sites on the coating enable secondary functional modifications.
- Pseudo-Mefp-5 universal coating exhibits great potential in biomedical applications.

REPORT

Mimicking *Mytilus edulis* foot protein: A versatile strategy for robust biomedical coatings

Zeyu Du,[1,2] Feng Qiao,[1] Liping Tong,[3] Wentai Zhang,[2] Xiaohui Mou,[1,2] Xin Zhao,[4] Manfred F. Maitz,[1,5] Huaiyu Wang,[3,6,*] Nan Huang,[2,7] and Zhilu Yang[1,2,*]

[1]School of Materials Science and Engineering, Department of Cardiology, Third People's Hospital of Chengdu Affiliated with Southwest Jiaotong University, Southwest Jiaotong University, Chengdu 610031, China

[2]Dongguan Key Laboratory of Smart Biomaterials and Regenerative Medicine, The Tenth Affiliated Hospital of Southern Medical University, Dongguan 523059, China

[3]Institute of Biomedicine and Biotechnology, Shenzhen Institute of Advanced Technology, Chinese Academy of Sciences, Shenzhen 518055, China

[4]Department of Biomedical Engineering, The Hong Kong Polytechnic University, Hung Hom, Hong Kong, China

[5]Max Bergmann Center of Biomaterials Dresden, Leibniz Institute of Polymer Research Dresden, Hohe Strasse 6, 01069 Dresden, Germany

[6]The Key Laboratory of Biomedical Imaging Science and System, Chinese Academy of Sciences, Shenzhen 518055, China

[7]GuangZhou Nanchuang Mount Everest Company for Medical Science and Technology, Guangzhou 510670, China

*Correspondence: hy.wang1@siat.ac.cn (H.W.); zhiluyang1029@swjtu.edu.cn (Z.Y.)

Received: March 27, 2024; Accepted: June 28, 2024; Published Online: June 29, 2024; https://doi.org/10.1016/j.xinn.2024.100671

Citation: Du Z., Qiao F., Tong L., et al., (2024). Mimicking *Mytilus edulis* foot protein: A versatile strategy for robust biomedical coatings. The Innovation **5(5)**, 100671.

Universal coatings with versatile surface adhesion, good mechanochemical robustness, and the capacity for secondary modification are of great scientific interest. However, incorporating these advantages into a system is still a great challenge. Here, we report a series of catechol-decorated polyallylamines (CPAs), denoted as pseudo-*Mytilus edulis* foot protein 5 (*pseudo*-Mefp-5), that mimic not only the catechol and amine groups but also the backbone of Mefp-5. CPAs can fabricate highly adhesive, robust, multifunctional polyCPA (PCPA) coatings based on synergetic catechol-polyamine chemistry as universal building blocks. Due to the interpenetrating entangled network architectures, these coatings exhibit high chemical robustness against harsh conditions (HCl, pH 1; NaOH, pH 14; H_2O_2, 30%), good mechanical robustness, and wear resistance. In addition, PCPA coatings provide abundant grafting sites, enabling the fabrication of various functional surfaces through secondary modification. Furthermore, the versatility, multifaceted robustness, and scalability of PCPA coatings indicate their great potential for surface engineering, especially for withstanding harsh conditions in multipurpose biomedical applications.

INTRODUCTION

Advances in surface coating technologies have driven the rapid development of chemical science, material science, and biomedical engineering.[1–4] Owing to substrate independence and versatile surface functionalization,[5] universal surface coatings are more attractive to practitioners in relevant fields. Current universal surface technologies include layer-by-layer (LBL) assembly,[6] chemical vapor deposition (CVD),[7] spin coating,[8,9] surface irradiation,[10] laser deposition,[11] and protein assembly.[12,13] However, there are still noticeable flaws in these systems. For instance, while LBL assembly and blood protein coatings offer scalability, they are susceptible to strong bases and acids.[14,15] Although coatings fabricated by surface irradiation, CVD, and laser deposition exhibit superior chemical resistance and adhesion, their applications are constrained by the substrate size and shape.[16,17] Spin coating is simple but offers weak substrate adhesion.[18] Consequently, these limitations narrow the scope of universal coatings for specific applications.

Mussels demonstrate exceptional adhesion to nearly all types of wet solid surfaces in marine environments.[19,20] Such adhesion capability relies on the secretion of *Mytilus edulis* foot proteins (Mefps), which form adhesive plaques via self-polymerization (Figures 1A–1C).[21] More surprisingly, mussel adhesive plaques maintain a strong and durable bond to solid substrates, even in harsh conditions, including extreme acidity, alkalinity, and oxidative environments (Figure S1). This unique adhesive property of plaques has inspired the emergence and development of polydopamine (PDA) coating, recognized as one of the most effective universal coating systems.[22–25] However, in contrast to the robustness of mussel adhesive plaques, PDA-based coatings exhibit limited mechanical strength, which may crack or detach under slightly harsh conditions (such as ultrasound, slight acidity, or alkalinity).[26–28] This is because the polymerization of PDA-based coatings mainly relies on the stacking of low-molecular-weight oligomers formed by catechol oxidation and self-polymerization. This forms a "concrete-like" structure devoid of a "skeleton-like" network that can "anchor" the oligomers.[29] Notably, Mefp-5, a linear macromolecule with an average molecular weight of ~10 kDa, plays a significant role in forming robust mussel adhesive plaques (Figure 1D).[30,31] As a flexible macromolecule containing catechol and amine groups, the crosslinking and entanglement of Mefp-5 during the self-polymerization process enable the formation of strong intermolecular and cohesive interactions among the backbone chains of the mussel adhesive plaque structure.[32–34] Based on this, we hypothesize that the coexistence of a chain-like backbone and functional groups (i.e., catechol and amine groups) is crucial for mussel adhesive plaque to achieve strong adhesion to a wide range of materials. The formed coatings provide a "reinforced concrete-like" structure, outstanding for mechanical and chemical robustness.

Here, inspired by the capability of Mefps to form a robust adhesive plaque, we develop a simple and versatile pseudo-Mefp-5 surface chemistry strategy for fabricating biomimetic, material-independent, and universal coatings with mechanical/chemical robustness and good scalability. To better mimic the backbone and functional groups of natural Mefp-5 (Figures 1E and 1F), catechol-modified polyamine (CPA; a pseudo-Mefp-5 molecule) was synthesized by conjugating hydrogenated caffeic acid (HCA) with polyallylamine (PA; molecular weight ~17 kDa). Through catechol-polyamine synergy, the CPA molecules can virtually form an interpenetrating entangled network structure with durable properties on all material surfaces (Figure 1G). The resulting polyPCA (PCPA) coatings exhibit exceptional chemical stability under extreme conditions, such as strong acids (HCl, pH 1), bases (NaOH, pH 14), and oxidants (H_2O_2, 30%), and can even withstand intense mechanical impact and severe deformation. Additionally, PCPA coatings are abundant with amine groups to support secondary reactions, enabling the creation of various functional surfaces. Importantly, the surface amine groups of PCPA coatings can be readily transformed into other reactive groups (e.g., carboxyl and bioclickable functional groups), facilitating further binding of bioactive molecules to expand the range of applications.[36,37] These tailored functionalities significantly enhance the practicality of the coatings, catering to the needs of various biomedical devices.[38–40] Due to robustness and scalability, PCPA coatings can be firmly formed on various biomaterials with multifunctional design, hence holding great potential for multipurpose surface engineering of advanced biomedical devices.

RESULTS AND DISCUSSION

Fabrication and characterization of PCPA coatings

Considering the critical role of the catechol-to-amine molar ratio of Mefp-5 in the formation of a robust adhesive plaque,[41,42] we prepared a series of CPAs with different degrees of HCA tethering onto PA (namely, the degree of substitution [DOS] of CPA) to explore the fabrication of robust coatings. To protect the phenolic hydroxyl groups of HCA from oxidation, the synthesis of CPA was performed under a biomimetic acidic anaerobic microenvironment, mimicking the environment in which mussels secrete Mefp-5. Following purification via dialysis, the synthesized CPA was characterized using nuclear magnetic resonance (NMR) and Fourier transform infrared (FTIR) spectroscopy. From the proton NMR (^{1}H-NMR) spectrum of CPA, the presence of diagnostic peaks, including the catecholic and aromatic protons of HCA, the amino protons of PA, and amide protons produced by amidation between the carboxyl groups of HCA and the

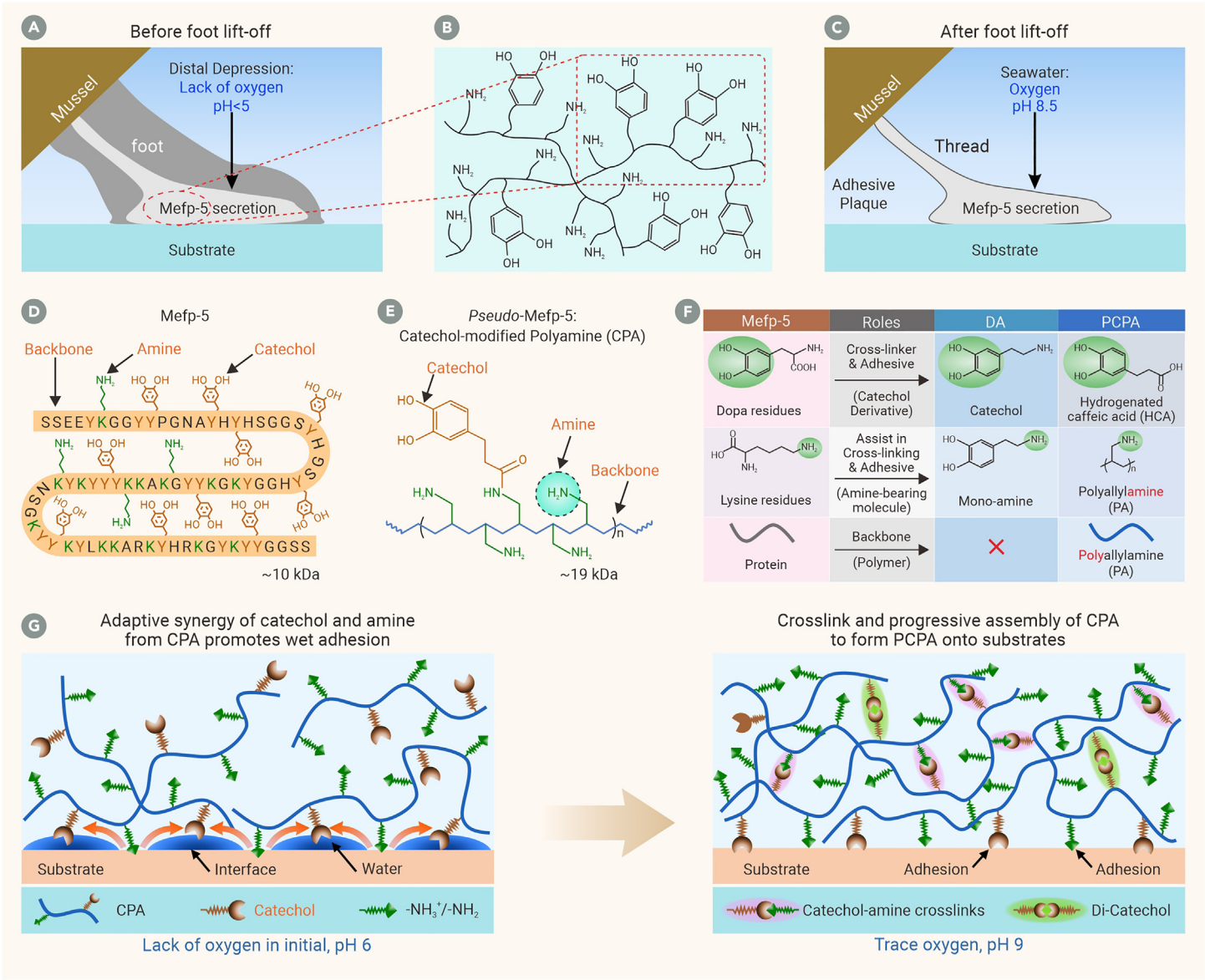

Figure 1. Pseudo-Mefp-5 surface chemistry strategy for fabricating catechol-polyamine-based robust coatings inspired by mussel adhesion plaques (A) Mussels secrete Mefp-5 to anchor to wet surfaces in an acidic and anaerobic microenvironment. (B) Simplified molecular schematic of Mefp-5. (C) Formation of a robust adhesive plaque triggered by Mefp-5 crosslinking onto wet surfaces under alkaline aerobic marine conditions. (D) The amino acid sequence of Mefp-5 (~10 kDa).[35] (E) Synthetic CPA (~19 kDa) containing both backbone and functional groups (i.e., amine and catechol groups) as a candidate cohesive polymers to mimic the structure of natural Mefp-5, used as macromolecular building blocks for fabricating robust coatings. (F) Sclerotization of the adhesive plaque based on the catechol-polyamine synergy of Mefp-5 (left) and the constituent analysis of PDA and PCPA coatings (right). (G) Schematics of CPA adhesion, crosslinking, and progressive assembly to form PCPA coatings on substrates inspired by mussel adhesive plaque formation.

amine groups of PA, indicated the tethering of HCA to PA (Figure S2A). Furthermore, FTIR analysis confirmed the successful synthesis of CPA, as evidenced by the good retention of the structures of both HCA (e.g., the peaks of Ar-OH, Ar-H, and aromatic C=C stretching vibrations at 3,350, 3,040, and 1,603 cm^{-1}, respectively) and PA (e.g., the peaks of -NH stretching vibrations at 3,360 and 3,290 cm^{-1}, respectively), the weak peak of -NH deformation vibrations at 1,585 cm^{-1}, and the emergence of new amide I and amide II peaks at 1,640 and 1,550 cm^{-1}, respectively (Figure S2B).

Next, UV-visible measurements were performed to determine the DOS of CPA (Figures S3A and S3B). Considering the 27 mol % of 3,4-dihydroxy-L-phenylalanine (DOPA) in Mefp-5,[43] CPA was synthesized with HCA and PA at different feed molar ratios of -COOH of the HCA to $-NH_2$ of the PA, ranging from 5% to 40%. The results indicated that the DOS of CPA was a function of the feed molar ratio and reached a value of up to 26.8% when the feed molar ratio was 40% (Figure S3C), close to the molar percentage of DOPA in Mefp-5. Correspondingly, the molecular weights of fabricated CPA with different DOS ranged from 17.3 to 21.2 kDa (Figure S3D).

We then explored the feasibility of the synthesized CPA for forming robust films. It was found that film formation strongly depended on (1) the pH value of the CPA solution and (2) the DOS of CPA. When the microenvironment turned from acidic (pH 6) and anaerobic to basic (pH 9) with a trace amount of oxygen, CPA could self-polymerize into a PCPA coating (Figures 1G and S4). At pH 9, the CPA with a DOS of 14.7% was the best for dip coating, with the fabricated PCPA coating showing a maximum surface amine group density of 15.3 nmol cm^{-2} (Figure S5). Moreover, scanning electron microscopy (SEM) and atomic force microscopy results indicated that a compact, homogeneous, and robust film was formed on the substrate after 24 h of dip coating (Figure S6). To illustrate the formation mechanism of PCPA coating, FTIR and X-ray photoelectron spectroscopy (XPS) measurements were carried out, indicating that CPA polymerization mainly involved catechol-amine chemical crosslinking reactions (i.e., Michael addition and Schiff base reactions between the amines and catechols of CPA) (Figures S7 and S8). Therefore, robust coatings with interpenetrating entangled network architectures could be fabricated by using this pseudo-Mefp-5 surface chemistry strategy (Figure S9).

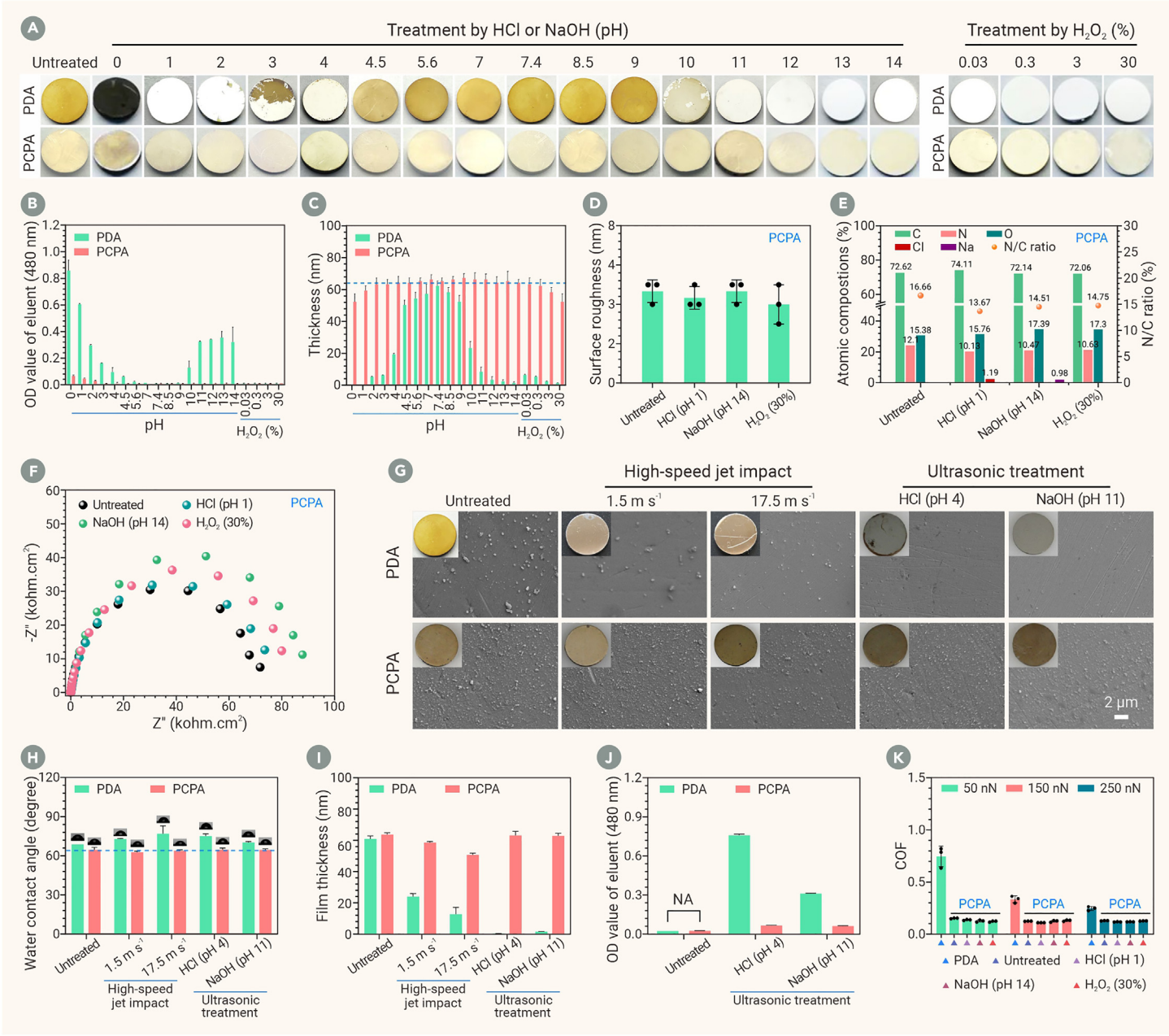

Figure 2. Chemical and mechanical robustness of PCPA coatings (A) Representative photos of the PDA- and PCPA-coated SS substrates before and after 24-h treatment with different chemical solutions. (B) OD values (at 480 nm) of the solutions after immersing the PDA- and PCPA-coated SS substrates for 24 h. (C) The thickness of the PDA and PCPA coatings after immersion in different chemical solutions for 24 h. (D) Changes in the roughness of the PCPA coatings before and after 24-h treatment with HCl (pH 1), NaOH (pH 14), or H_2O_2 (30%) were determined by 3D profiling. (E) Chemical compositions of the PCPA coatings before and after 24-h treatment with HCl (pH 1), NaOH (pH 14), or H_2O_2 (30%). (F) Electrochemical impedance spectra of the PCPA-coated substrates before and after 24-h treatment with HCl (pH 1), NaOH (pH 14), or H_2O_2 (30%), measured in 10 mM PBS solution (pH 7.4) at 37°C. (G) Morphology of the PDA and PCPA coatings before and after exposure to high-speed water impacts and ultrasound treatment (pH 4 or 11). (H) Hydrophilicity of the PDA and PCPA coatings before and after exposure to high-speed water impacts and ultrasound treatment (pH 4 or 11). (I) Film thickness of the PDA and PCPA coatings before and after exposure to high-speed water impacts and ultrasound treatment (pH 4 or 11). (J) OD values (at 480 nm) of the solutions with PDA and PCPA-coated SS substrates after ultrasound treatment (pH 4 or 11) for 4 h. NA indicates the absence of significant absorbance values. (K) COF of the PDA and PCPA coatings under different loads before and after the treatment with HCl (pH 1), NaOH (pH 14), or H_2O_2 (30%). n = 3. All error bars are mean ± SD.

Subsequently, the versatility of our pseudo-Mefp-5 surface chemistry strategy was verified by coating PCPA films onto 12 different substrates, including noble metal (Au) components, metals with native oxide surfaces (a stainless steel [SS] substrate and biomedical device and an NiTi shape-memory alloy), oxide (TiO_2), nitride (Ti_3N_4), mineral (Si), ceramic (glass), and polymers (polyvinyl chloride [PVC], polytetrafluoroethylene [PTFE], polystyrene, polyethylene terephthalate, and polyurethane [PU]) (Figure S10). Although a single cycle of dip coating resulted in an incomplete coating for some substrates (e.g., Au, NiTi, PVC, and PTFE), a homogeneous coating was achieved for all other studied substrates after three cycles of dip coating. Additionally, all modified samples showed noticeable color changes (Figure S11A), and their surface amine densities increased with the dip coating cycles (Figure S11B). Thus, PCPA coatings could be obtained at an optimized feed concentration of CPA with 3 cycles of dip coating: robust, compact, and homogeneous (Figures S11C and S11D).

Chemical and mechanical robustness of PCPA coatings

The insufficient chemical robustness of surface coating is a significant obstacle to their real-world application.[44] Here, we assessed the resistance of PCPA coatings to harsh chemical conditions using a strong acid (HCl), strong base (NaOH), and strong oxidant (H_2O_2). The traditional mussel-inspired PDA coating (merely mimicking the catechol groups of Mefp-5) was set as a control. As depicted in Figure 2A, at a pH below 4 and above 10, the PDA coatings exhibited a lighter and uneven color, suggesting thinning and detachment of the coating. Furthermore, after treatment with varying concentrations of H_2O_2, the

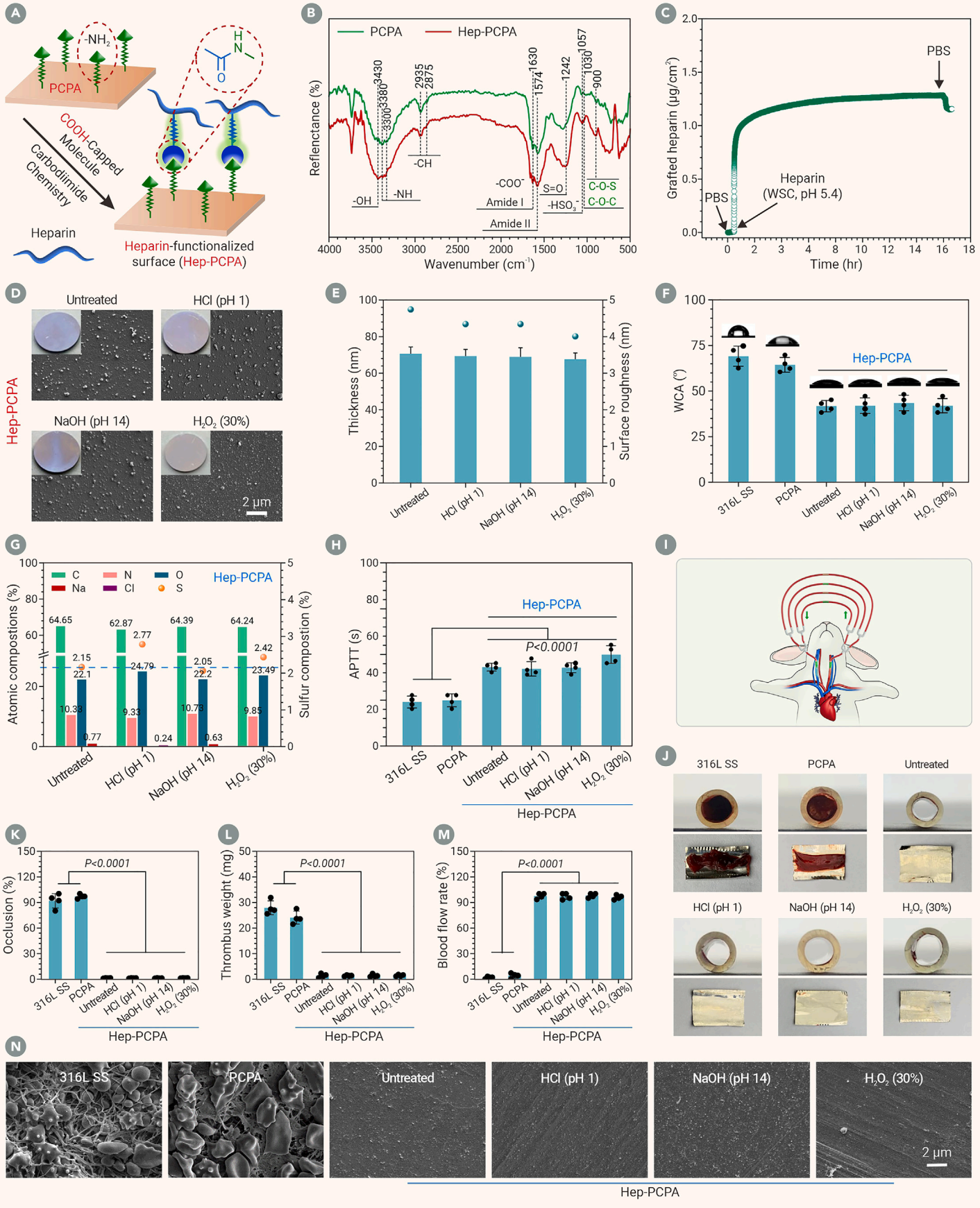

Figure 3. Secondary covalent immobilization of heparin onto PCPA coatings for developing durable antithrombotic surfaces (A) Schematic of heparin conjugation to PCPA-coated surfaces. (B) FTIR spectra of the PCPA-coated surfaces before and after heparin grafting. (C) Real-time analysis of the heparin grafting process by quartz crystal microbalance equipped with dissipation monitoring (QCM-D). (D) Macroscopic photos and SEM images of the Hep-PCPA-coated surfaces before and after treatment with HCl (pH 1), NaOH (pH 14),

(legend continued on next page)

substrate beneath was fully exposed, indicating complete detachment of the coating (Figure S12). The poor chemical stability of PDA coatings can be attributed to their inherent intermolecular interactions, including hydrogen bonds, π-π stacking, and cation-π interactions, which are susceptible to strong chemicals.[29,45,46] In contrast, PCPA coatings showed excellent chemical robustness and could maintain their integrity after treatment with HCl (except pH 0), NaOH, or H_2O_2. Note that the undetected optical density (OD) values for the PDA groups after treatment with H_2O_2 were probably due to the disruption of cyclic structures in the dopamine oligomers (Figure 2B).[47,48] Moreover, little changes were observed in film thickness (Figure 2C), surface roughness (Figure 2D), surface topography (Figure S13), and chemical composition (Figure 2E) for the PCPA coatings, further confirming their chemical robustness. The electrochemical impedance of the PCPA-coated substrates following HCl, NaOH, or H_2O_2 treatment was also measured. As shown in Figure 2F, there was only a slight increase in the impedance value of PCPA coatings after different treatments. Thus, all of these results strongly demonstrated the excellent chemical robustness of PCPA coatings in harsh chemical conditions.

In addition to chemical robustness, mechanical robustness is crucial for practical applications of surface coatings. Therefore, we gauged the mechanical robustness of PCPA coatings utilizing continuous water jet impacts and ultrasonic vibrations (Figure 2G). Notably, the PCPA coatings showcased consistent morphology after 4 h of continuous water washing (1.5 m s^{-1}). Still, after the same treatment, the change in PDA coatings was visible to the naked eye. Both kinds of coatings were then exposed to higher-speed water jet impacts (17.5 m s^{-1}) for 1 h and revealed that the surface morphology, and hydrophilicity of PCPA coatings were almost undamaged post impact (Figure 2H). To assess the resistance of different coatings to physical dissociation, the samples were further subjected to high-frequency ultrasonic treatment at acidic (pH 4) or basic (pH 11) conditions for up to 4 h. While the PDA coatings faltered and detached from the substrate, as evidenced by film thickness and significant shifts in the OD value of eluent (Figures 2I and 2J), the stability of PCPA coatings under such harsh conditions was satisfactory. Tribological testing indicated the superior frictional resilience of PCPA coatings, of which the coefficient of friction (COF) was consistent after different treatments and much lower than that of PDA coatings (Figure 2K). For biomedical devices, the mechanical integrity of coatings is one of the primary evaluation indicators. We hence selected cardiovascular stents, a biomedical device that should endure intense deformation during clinical application, to evaluate the tenacity of PCPA coatings. Our analysis, backed by macroscopic photos and SEM images, highlighted a consistent and smooth PCPA coating on the 316L SS stent (Figure S14). Following balloon dilation, the coatings on the stent remained unscathed, verifying their excellent adhesion and deformation resilience. Conclusively, pseudo-Mefp-5 surface chemistry is a strategy worth advocating for constructing universal coatings. Such coatings are substrate independent and are promising for robust defense against chemical and mechanical challenges.

PCPA coatings to attain a durable functional surface

The durability of functional surfaces is crucial for the long-term service of biomedical implants. Given the potent robustness and abundant amine groups of the pseudo-Mefp-5 PCPA coatings, we examined the durability and scalability of this surface coating strategy. In particular, accelerated durability tests of functional coatings following harsh treatment with HCl (pH 1), NaOH (pH 14), or H_2O_2 (30%) were designed to shorten the experimental time. Due to the abundant amine groups, PCPA coatings could be readily functionalized with carboxyl-bearing biomolecules through water-soluble carbodiimide chemistry (Figure 3A). For example, an antithrombotic surface was fabricated via the covalent immobilization of heparin, one of the most commonly used anticoagulant drugs for blood-contacting devices. A series of surface characterizations were also carried out to elucidate the chemical changes of PCPA coating after heparin grafting. As shown in Figure 3B, the significant increases in the intensities of the peaks at 1,242, 1,030, and 900 cm^{-1} and the new peaks at 3,430 and 1,057 cm^{-1} indicated the introduction of S=O, C-O-C, C-O-S, -OH, and -HSO_3^- derived from heparin, suggesting the successful immobilization of heparin onto the PCPA coatings. Furthermore, XPS analysis confirmed the grafting of heparin (sodium salt), as evidenced by the emergence of S and Na peaks in the spectrum (Figure S15) and the remarkable changes in the chemical compositions (Figure S16; Table S1). Moreover, the heparin-grafting efficacy of pseudo-Mefp-5 PCPA coatings was up to ~1.2 μg cm^{-2} (Figure 3C), considerably higher than that of most available methods.[49]

Next, the influence of harsh chemical solutions, including HCl (pH 1), NaOH (pH 14), and H_2O_2 (30%), on various surface properties of heparinized PCPA (Hep-PCPA) coatings were evaluated. SEM and 3D profilometry revealed that these harsh treatments slightly changed the surface morphology of Hep-PCPA coatings (Figures 3D and S17), leading to slight decreases in surface roughness, film thickness, and surface hydrophilicity (Figures 3E and 3F). Meanwhile, the changes in surface chemical compositions were inconspicuous, and no weakening effects on the surface sulfur content could be found (Figures 3G, S18, and S19; Table S2). As a simple and reliable method for measuring blood coagulation, the activated partial thromboplastin time (APTT) assay is commonly used to test the bioactivity of heparin bound to surfaces.[50] In this study, the APTT of Hep-PCPA-coated surfaces was prolonged for ~16 s compared to that of bare 316L SS and PCPA-coated surfaces, which was almost unchanged after treatment with HCl (pH 1), NaOH (pH 14), or H_2O_2 (30%) (Figure 3H). All of these results demonstrated the robust tethering and bioactivity retention of immobilized heparin.

Furthermore, we tested the anticoagulation properties of Hep-PCPA coatings before and after treatment with HCl (pH 1), NaOH (pH 14), or H_2O_2 (30%) using *ex vivo* blood circulation using the New Zealand white rabbit arteriovenous shunt model (Figure 3I). Compared to Hep-PCPA, 316L SS and PCPA-modified samples were entirely blocked by occlusive thrombosis after 2 h of blood circulation (Figures 3J–3M). Additionally, SEM analysis revealed that thrombi formed on both the bare and PCPA-coated surfaces consisted of fibrin networks filled with red blood cells and activated platelets. In contrast, almost no fibrin network, red blood cells, or platelets were observed on Hep-PCPA coatings (Figure 3N). These results confirmed the successful development of robust anti-thrombogenic surfaces by fabricating pseudo-Mefp-5 PCPA coatings, which were superior to those obtained by the existing methods for heparin immobilization.[51,52] We believe that this antithrombogenic coating strategy has great application potential, as it can be readily used to functionalize the blood-contacting materials/biomedical devices for the long-term and effective prevention of thrombosis.

Conversion of the functional groups of PCPA coatings for attaining multitype grafted molecules

The PCPA coatings were also versatile in converting its abundant surface amine groups into other reactive functional groups (e.g., carboxyl and clickable functional groups), which could support secondary reactions for expanding applications.

Conversion of the surface amine groups of PCPA coatings into carboxyl groups enabling the grafting of amine-bearing molecules. As a proof of concept, we first employed succinic anhydride (SA) to convert the surface amine groups of PCPA coatings into carboxyl groups (Figure 4A). This was accomplished by immersing the PCPA-coated samples in SA solution at room temperature overnight. FTIR spectroscopy analysis revealed that the N-H stretching peak of amine groups at ~3,250 cm^{-1} was substantially attenuated in the spectrum of SA-tethered PCPA (SA-PCPA) coatings when two new broad peaks appeared at ~3,350 and 1,720 cm^{-1}, attributed to the O-H and C=O stretching of carboxyl groups (Figure 4B, red). Moreover, the intensity of the C=O stretching peak at ~ 1,640 cm^{-1} increased significantly, indicating the production of a new amido bond. Together, these results demonstrated the successful introduction of carboxyl groups onto PCPA coatings through the one-step carbodiimide

and H_2O_2 (30%) for 24 h. (E) Changes in surface thickness and roughness. (F) Changes in surface hydrophobicity. (G) Surface chemistry of the Hep-PCPA coatings before and after treatment with HCl (pH 1), NaOH (pH 14), or H_2O_2 (30%) for 24 h. (H) APTT values of the Hep-PCPA-coated surfaces before and after treatment with HCl (pH 1), NaOH (pH 14), or H_2O_2 (30%) for 24 h. (I) Schematic of the New Zealand white rabbit arteriovenous shunt model. (J) Cross-sectional photographs of tubes installed with bare 316L SS foils, PCPA-coated 316L SS foils, and Hep-PCPA-coated 316L SS foils before and after treatment with HCl (pH 1), NaOH (pH 14), or H_2O_2 (30%), exposed to blood flow without anticoagulant for 2 h and photographs of thrombi formed on different surfaces. (K) Occlusion rates of tubes installed with various samples after 2 h of blood circulation. (L) Quantitative results of the thrombus weight. (M) Retention of the blood flow rate of different samples within circuits after continuous blood circulation for 2 h. (N) Thrombus composition evaluated by SEM. $n = 4$. Comparisons between more than two groups were analyzed by one-way ANOVA. Statistically significant differences are shown as $^{****}p < 0.0001$. All error bars are mean ± SD.

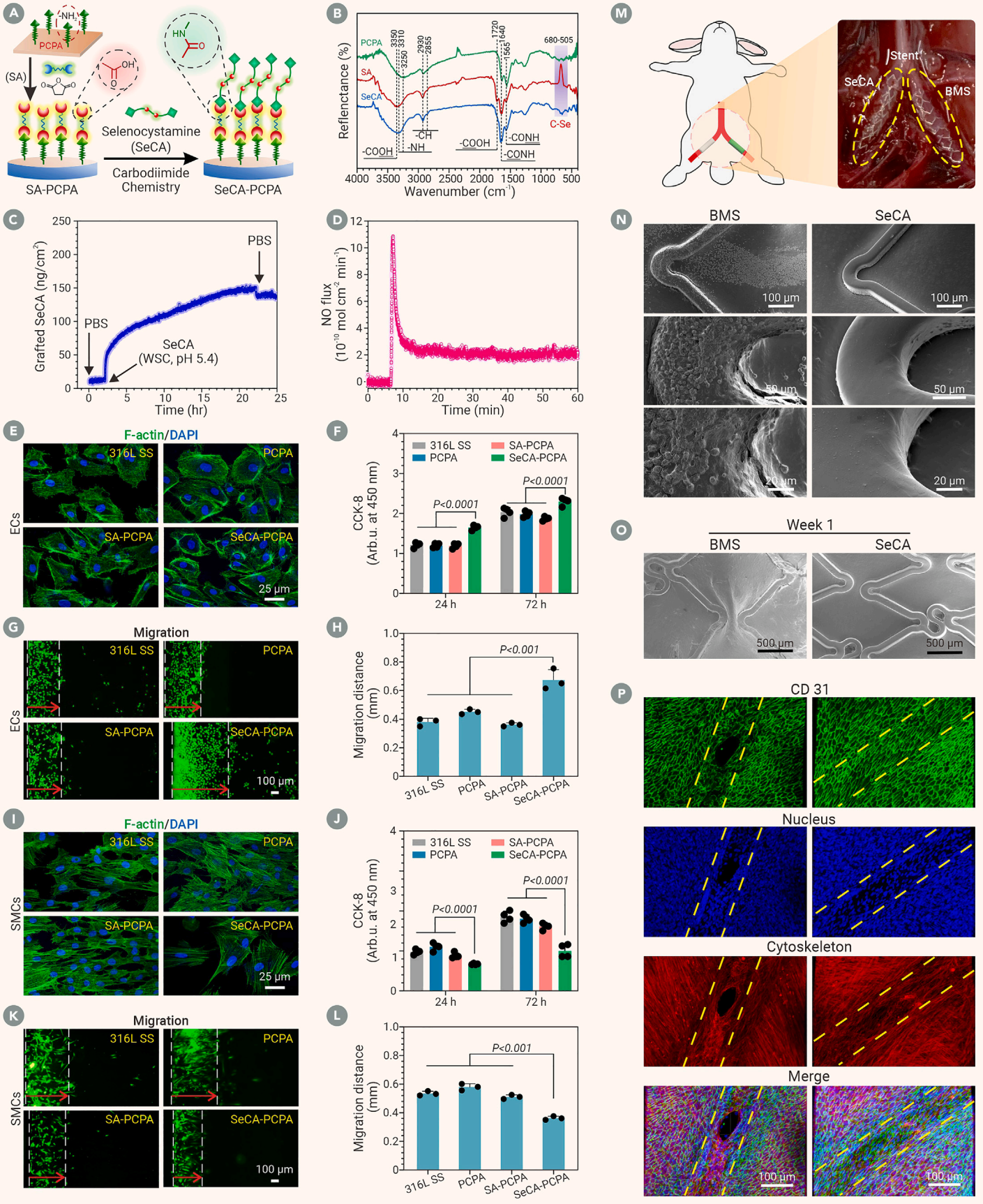

Figure 4. Surface carboxylation of the PCPA coatings enabling the grafting of amine-bearing molecules (A) Schematic of the conversion of surface amine groups of the PCPA coatings into carboxyl groups for the covalent immobilization of the amine-bearing SeCA. (B) FTIR spectra of PCPA-coated surfaces before and after carboxylation and further covalent immobilization of SeCA. (C) Real-time QCM-D analysis of the grafting process of SeCA onto the SA-PCPA surfaces. (D) NO catalytic generation of SeCA-PCPA coatings. (E–H)

(legend continued on next page)

immobilization of SA. Acid orange II and toluidine blue staining[53] was performed to determine the surface density of the amine and carboxyl groups before and after SA grafting. The results revealed that SA grafting substantially reduced the density of amine groups (Figure S20A). In contrast, a carboxyl group density of ~25.1 nmol cm^{-2} was measured on the SA-tethered surfaces (Figure S20B), indicating the efficient conversion of the surface amine groups (~27.3 nmol cm^{-2}) of PCPA coatings into carboxyl groups.

To confirm the ability of the introduced carboxyl groups to tether bioactive molecules, an amine-bearing molecule, selenocystamine (SeCA) was employed for the secondary modification of SA-PCPA coatings. FTIR spectroscopy analysis revealed a remarkable increase of the peaks at approximately 505–680 cm^{-1} (Figure 4B, blue), suggesting the introduction of C-Se derived from SeCA. Moreover, XPS analysis further confirmed the successful immobilization of SeCA, as evidenced by the presence of the Se signal in the spectrum of SeCA-PCPA coatings (Figure S21) and the significant changes in surface chemical compositions (Table S3). Furthermore, the quartz crystal microbalance equipped with dissipation monitoring (QCM-D) result revealed that ~140 ng cm^{-2} SeCA was bound to the SA-PCPA-coated surfaces (Figure 4C).

As an organoselenium species, SeCA has glutathione peroxidase-like catalytic activity and can generate nitric oxide (NO) from S-nitrosothiols. This property of SeCA has been widely used to develop NO-generation materials.[54] Here, a real-time chemiluminescence assay was carried out to investigate the catalytic release of NO by SeCA-PCPA-functionalized 316L SS substrates in PBS solution (pH 7.4) containing 30 μM S-nitroso-N-acetyl-DL-penicillamine and 30 μM glutathione. As shown in Figure 4D, SeCA-PCPA catalyzed NO release at a stable release rate under physiological conditions (~2.2 × 10^{-10} mol cm^{-2} min^{-1}).[55,56] More importantly, owing to the chemical robustness of PCPA coatings, the surface-bound SeCA showed a highly durable capability of catalytic NO generation. Approximately 76% of the initial NO release rate was detected after continuous exposure of the SeCA-PCPA-functionalized 316L SS substrates to NO donor solution for up to 30 days (Figure S22). Given the pivotal role of NO in the cardiovascular system, the effect of SeCA-PCPA coating on different vascular cells was further assessed. As shown in Figures 4E–4L, SeCA-PCPA coatings could significantly enhance the proliferation and migration of endothelial cells (ECs) while inhibiting the excessive proliferation and migration of smooth muscle cells (SMCs). This indicates that the SeCA-PCPA functionalized coating can regulate the behaviors of different vascular cells through the continuous and stable catalytic release of NO. Subsequently, we implanted bare metal stents (BMSs) and SeCA-PCPA-coated stents into the bilateral iliac arteries of New Zealand white rabbits to further assess their biological performances *in vivo* (Figure 4M). As shown in Figure 4N, without using any anticoagulants, BMSs were significantly enveloped by blood cells 2 h post implantation. In contrast, the surface structure of SeCA-PCPA-coated stents remained distinctly visible, with blood components that were hardly found. This finding confirms that the SeCA-PCPA coating significantly enhances the anti-thrombogenic performance of implanted devices in a blood environment. 1 week post implantation, the structural contours of SeCA-PCPA-treated stents were clearer than those of BMSs (Figure 4O). Moreover, immunofluorescent staining revealed that the surface of SeCA-PCPA-coated stents was fully covered by CD 31-positive ECs 1 week post implantation (Figure 4P). Evidently, the fabricated robust SeCA-PCPA coatings can prevent thrombosis formation and facilitate the repair of damaged blood vessels *in vivo*.

Conversion of the surface amine groups of PCPA coatings into clickable functional groups for "clean" molecular modification. Carbodiimide chemistry is one of the most popular chemical coupling strategies, and it has been widely used for covalently immobilizing bioactive molecules onto material surfaces.[57] However, carbodiimide chemistry for grafting molecules containing primary amine and carboxyl groups (e.g., peptides, proteins, and growth factors) inevitably leads to chemical crosslinking among the molecules and reduces their bioactivity.[58] Additionally, carbodiimide chemistry has low efficiency and specificity, undermining the controllability and reproducibility of molecule immobilization. As an alternative, bioorthogonal click chemistry (e.g., azide-dibenzylcyclooctyne (azide-DBCO) cycloaddition) has attracted widespread interest recently due to its unique advantages, including rapidity, specificity, selectivity, thoroughness, and biocompatibility.[59–62] Notably, bioorthogonal click chemistry has been widely applied for molecular conjugation,[63] with distinct superiority in immobilizing peptides on material surfaces.[64–68] Thus, the conversion of the surface amine groups of PCPA coating into clickable functional groups was proposed here to develop an advanced surface bioengineering strategy for "clean" molecular modification.

To this end, an NHS-functionalized azide-bearing molecule (NHS-PEG_4-azide; Figure 5A) was immobilized onto PCPA-coated PU (one of the most popular materials for fabricating medical tubes) based on NHS-NH_2 carbodiimide chemistry. Afterward, a customized DBCO-modified antibacterial peptide (DBCO-ABP) was synthesized (Figures 5B, S23, and S24) and grafted onto the samples via bioorthogonal click chemistry (Figure 5C). The antibacterial function was selected as it was a general requirement of biomedical devices, including medical tubes.[40] As shown in Figure 5D, a new peak at ~2,106 cm^{-1} was assigned to the -N=N^+=N^- stretching of azide groups. The peaks of C=O (at ~1,665 cm^{-1}) and C-O-C (at ~1,067 cm^{-1}) were also detected, indicating the successful conjugation of NHS-PEG_4-azide through the NHS-NH_2 carbodiimide reaction. Following the surface grafting of DBCO-ABP, the -N=N^+=N^- stretching peak of azide groups at ~2,106 cm^{-1} disappeared, confirming the effective click reaction between DBCO groups and azide groups. QCM-D measurement revealed that ~520 and ~360 ng cm^{-2} of NHS-PEG_4-azide and DBCO-ABP were immobilized onto the PCPA coatings and the azide-functionalized surfaces (Figures 5E and 5F), respectively. Importantly, it indicated the effective conversion of surface amine groups into clickable functional groups, enabling the bioorthogonal click grafting of peptides.

To assess the efficacy of ABP-PCPA-coated PU in preventing bacterial colonization, 2 bacterial strains (*E. coli* as gram-negative bacteria and *S. epidermidis* as gram-positive bacteria), commonly associated with catheter infection, were utilized for the following study. The results of the plate counting assay showed that the ABP-PCPA coatings could sterilize 98.7% of *E. coli* and 99.7% of *S. epidermidis* compared to the PU samples (Figures 5G and 5H). To investigate the effect on host inflammatory response, the PU and ABP-PCPA-coated PU catheters were exposed to *E. coli* or *S. epidermidis* and then subcutaneously implanted in the backs of healthy rats for 5 days (Figure 5I). The results showed that severe inflammation occurred on the surface of pristine PU catheters, which could be attributed to bacterial infection (Figure 5J). In contrast, the ABP-PCPA-coated PU catheters exhibited a 34.8% reduction of inflammation against *E. coli* invasion and a 44.33% reduction of inflammation against *S. epidermidis* invasion, respectively (Figure 5K). Collectively, our results demonstrated the superiority of PCPA coatings in developing an advanced bioorthogonal clickable surface engineering strategy for "clean" molecular modification. Moreover, the bioactivity of the grafted molecules is well retained.

CONCLUSION

In summary, inspired by the crucial role of the coexistence of the backbone and catechol and amine groups of Mefp-5 in forming robust mussel adhesive plaques, we developed a pseudo-Mefp-5 surface chemistry strategy for fabricating universal coatings with excellent robustness and scalability. Using a catechol-modified PA that mimics the functional groups and backbone of Mefp-5, coatings with an interpenetrating network that show good adhesive strength to various materials are developed. Thus, these features impart the coated substrates or biomedical devices (e.g., cardiovascular stents and central venous catheters) with high chemical robustness against strong acids, bases, and oxidants and mechanical robustness against friction and deformation. Furthermore, the pseudo-Mefp-5 coatings can be decorated with abundant and different reactive functional groups to covalently tether various bioactive molecules to develop multi-purpose surfaces. In conclusion, the pseudo-Mefp-5 surface chemistry strategy proposed in this study is far superior to other surface techniques and toolkits and is simple, effective, and versatile enough for the surface functionalization of various biomedical materials/devices with multipurpose applications.

Confocal laser-scanning microscope (CLSM) images of ECs stained with F-actin (green) and DAPI (blue) (E), cell viability (F), migration images (G), and quantification of migration distance (H). (I–L) CLSM images of SMCs stained with F-actin (green) and DAPI (blue) (I), cell viability (J), migration images (K), and quantification of migration distance (L). (M) Schematic of iliac artery stent implantation in New Zealand white rabbits. (N) SEM images of different stents 2 h post implantation *in vivo*. (O and P) SEM (O) and CLSM (P) images of different stents 1 week post implantation *in vivo*. The area between the white dashed lines represents the stent struts. $n = 4$. Comparisions between more than two groups were analyzed by one-way ANOVA. Statistically significant differences are shown as ***$p < 0.001$ and ****$p < 0.0001$. All error bars are mean ± SD.

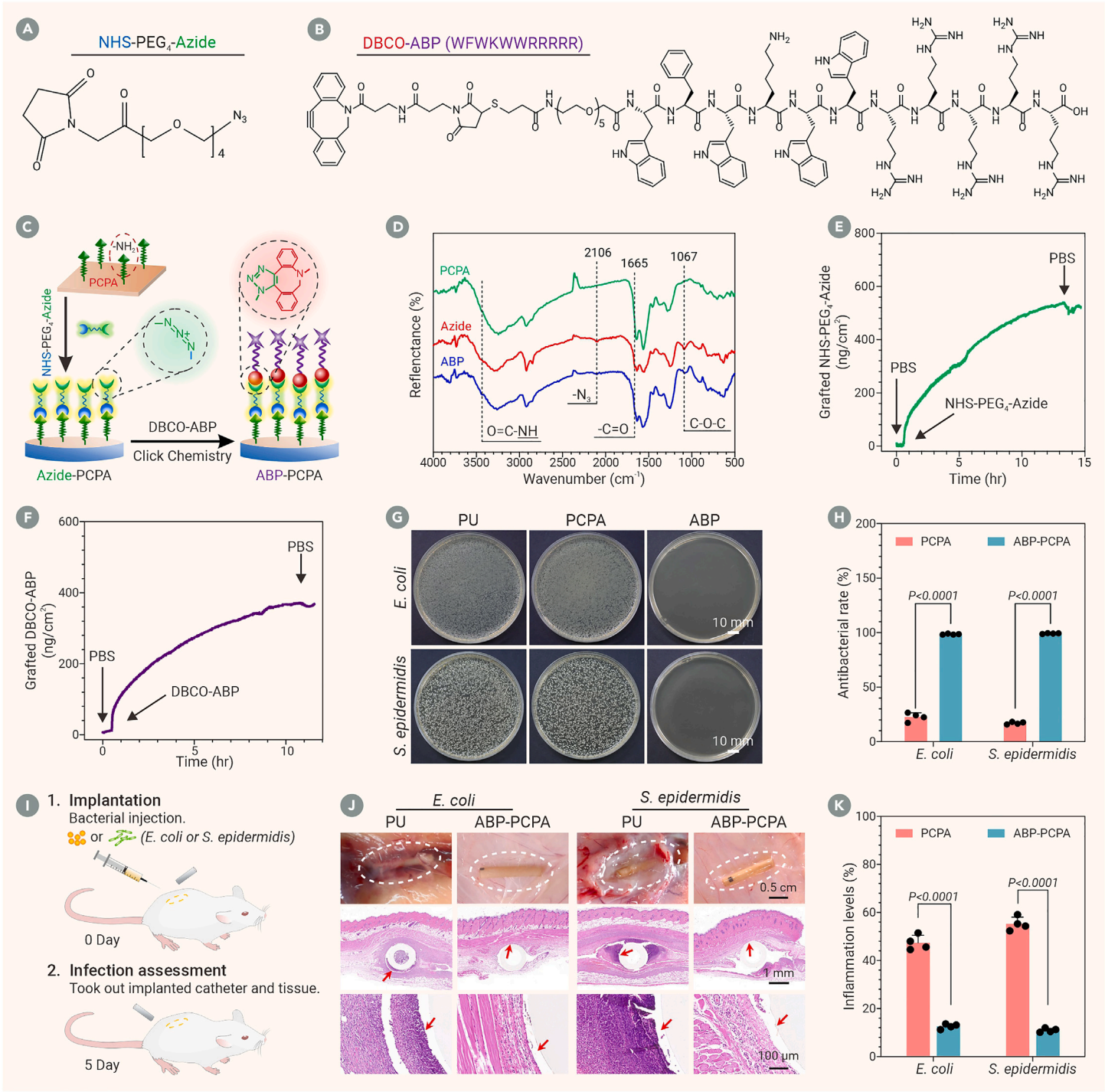

Figure 5. Surface azidation of the PCPA coatings for "clean" molecular modification (A) Chemical structure of NHS-PEG$_4$-azide and (B) DBCO-ABP (WFWKWWRRRRR). (C) Schematic of converting surface amine groups of PCPA coatings into azide groups for the click grafting of DBCO-ABP. (D) FTIR spectra of PCPA-coated substrates before and after surface azidation and further click grafting of DBCO-ABP. (E) Real-time QCM-D analysis of the grafting process of NHS-PEG$_4$-azide on the PCPA-coated surfaces. (F) Real-time QCM-D analysis of the grafting process of DBCO-ABP on the azide-functionalized surfaces. (G) Representative colony images of *E. coli* and *S. epidermidis* after incubating on different surfaces for 24 h. (H) Antibacterial rates of different surfaces against *E. coli* and *S. epidermidis*. (I) Schematic of subcutaneous implantation in rats. (J) Macroscopic images and H&E staining images of the implantation sites 5 days post implantation *in vivo*, with red arrows indicating the implants. (K) Quantitative analysis of the peri-implantation inflammation levels. n =4. Comparisions between more than two groups were analyzed by one-way ANOVA. Statistically significant differences are shown as ****$p < 0.0001$. All error bars are mean ± SD.

MATERIALS AND METHODS

See supplemental information for details.

REFERENCES

1. Zhang, Y., Zheng, F., Yang, T., et al. (2012). Tuning the autophagy-inducing activity of lanthanide-based nanocrystals through specific surface-coating peptides. Nat. Mater. ***11***(9): 817–826. https://doi.org/10.1038/nmat3363.
2. Zhi, D., Cheng, Q., Midgley, A.C., et al. (2022). Mechanically reinforced biotubes for arterial replacement and arteriovenous grafting inspired by architectural engineering. Sci. Adv. ***8***(11): eabl3888. https://doi.org/10.1126/sciadv.abl3888.
3. Zhang, T., Liu, N., Xu, J., et al. (2023). Flexible electronics for cardiovascular healthcare monitoring. Innovation ***4***(5): 100485. https://doi.org/10.1016/j.xinn.2023.100485.
4. Du, J., and Feng, X.-Q. (2024). Biomedical microrobotics: Small sizes, large applications. Innov. Life ***2***(1): 100046. https://doi.org/10.59717/j.xinn-life.2024.100046.
5. Wei, Q., and Haag, R. (2015). Universal polymer coatings and their representative biomedical applications. Mater. Horiz. ***2***(6): 567–577. https://doi.org/10.1039/C5MH00089K.
6. Matosevic, S., and Paegel, B.M. (2013). Layer-by-layer cell membrane assembly. Nat. Chem. ***5***(11): 958–963. https://doi.org/10.1038/nchem.1765.
7. Alf, M.E., Asatekin, A., Barr, M.C., et al. (2010). Chemical vapor deposition of conformal, functional, and responsive polymer films. Adv. Mater. ***22***(18): 1993–2027. https://doi.org/10.1002/adma.200902765.

8. Mitzi, D.B., Kosbar, L.L., Murray, C.E., et al. (2004). High-mobility ultrathin semiconducting films prepared by spin coating. Nature ***428***(6980): 299–303. https://doi.org/10.1038/nature02389.
9. Zhao, W., Yan, Y., Chen, X., et al. (2022). Combining printing and nanoparticle assembly: Methodology and application of nanoparticle patterning. Innovation ***3***(4): 100253. https://doi.org/10.1016/j.xinn.2022.100253.
10. Peng, B., Locascio, M., Zapol, P., et al. (2008). Measurements of near-ultimate strength for multiwalled carbon nanotubes and irradiation-induced crosslinking improvements. Nat. Nanotechnol. ***3***(10): 626–631. https://doi.org/10.1038/nnano.2008.211.
11. Xiao, J., Liu, P., Wang, C., et al. (2017). External field-assisted laser ablation in liquid: An efficient strategy for nanocrystal synthesis and nanostructure assembly. Prog. Mater. Sci. ***87***(2017): 140–220. https://doi.org/10.1016/j.pmatsci.2017.02.004.
12. Okesola, B.O., and Mata, A. (2018). Multicomponent self-assembly as a tool to harness new properties from peptides and proteins in material design. Chem. Soc. Rev. ***47***(10): 3721–3736. https://doi.org/10.1039/c8cs00121a.
13. Zhu, J., Avakyan, N., Kakkis, A., et al. (2021). Protein assembly by design. Chem. Rev. ***121***(22): 13701–13796. https://doi.org/10.1021/acs.chemrev.1c00308.
14. Yang, P., Zhu, F., Zhang, Z., et al. (2021). Stimuli-responsive polydopamine-based smart materials. Chem. Soc. Rev. ***50***(14): 8319–8343. https://doi.org/10.1039/d1cs00374g.
15. Luo, Q., Hou, C., Bai, Y., et al. (2016). Protein assembly: versatile approaches to construct highly ordered nanostructures. Chem. Rev. ***116***(22): 13571–13632. https://doi.org/10.1021/acs.chemrev.6b00228.
16. Yan, Z., Peng, Z., and Tour, J.M. (2014). Chemical vapor deposition of graphene single crystals. Acc. Chem. Res. ***47***(4): 1327–1337. https://doi.org/10.1021/ar4003043.
17. Coclite, A.M., Howden, R.M., Borrelli, D.C., et al. (2013). 25th anniversary article: CVD polymers: a new paradigm for surface modifi cation and device fabrication. Adv. Mater. ***25***(38): 5392–5423. https://doi.org/10.1002/adma.201301878.
18. Kelso, M.V., Mahenderkar, N.K., Chen, Q., et al. (2019). Spin coating epitaxial films. Science ***364***(6436): 166–169. https://doi.org/10.1126/science.aaw6184.
19. Cha, H.J., Hwang, D.S., and Lim, S. (2008). Development of bioadhesives from marine mussels. Biotechnol. J. ***3***(5): 631–638. https://doi.org/10.1002/biot.200700258.
20. Maier, G.P., Rapp, M.V., Waite, J.H., et al. (2015). BIOLOGICAL ADHESIVES. Adaptive synergy between catechol and lysine promotes wet adhesion by surface salt displacement. Science ***349***(6248): 628–632. https://doi.org/10.1126/science.aab0556.
21. Danner, E.W., Kan, Y., Hammer, M.U., et al. (2012). Adhesion of mussel foot protein Mefp-5 to mica: an underwater superglue. Biochemistry ***51***(33): 6511–6518. https://doi.org/10.1021/bi3002538.
22. Lynge, M.E., van der Westen, R., Postma, A., et al. (2011). Polydopamine-a nature-inspired polymer coating for biomedical science. Nanoscale ***3***(12): 4916–4928. https://doi.org/10.1039/c1nr10969c.
23. Liebscher, J.r., Mrówczyński, R., Scheidt, H.A., et al. (2013). Structure of polydopamine: a never-ending story? Langmuir ***29***(33): 10539–10548. https://doi.org/10.1021/la4020288.
24. Han, L., Lu, X., Liu, K., et al. (2017). Mussel-inspired adhesive and tough hydrogel based on nanoclay confined dopamine polymerization. ACS Nano ***11***(3): 2561–2574. https://doi.org/10.1021/acsnano.6b05318.
25. Lee, H., Dellatore, S.M., Miller, W.M., et al. (2007). Mussel-inspired surface chemistry for multifunctional coatings. Science ***318***(5849): 426–430. https://doi.org/10.1126/science.1147241.
26. Yang, W., Liu, C., and Chen, Y. (2018). Stability of polydopamine coatings on gold substrates inspected by surface plasmon resonance imaging. Langmuir ***34***(12): 3565–3571. https://doi.org/10.1021/acs.langmuir.7b03143.
27. Schlaich, C., Li, M., Cheng, C., et al. (2018). Mussel-inspired polymer-based universal spray coating for surface modification: fast fabrication of antibacterial and superhydrophobic surface coatings. Adv. Mater. Interfac. ***5***(5): 1701254. https://doi.org/10.1002/admi.201701254.
28. Mao, S., Zhang, D., Zhang, Y., et al. (2020). A universal coating strategy for controllable functionalized polymer surfaces. Adv. Funct. Mater. ***30***(40): 2004633. https://doi.org/10.1002/adfm.202004633.
29. Hong, S., Wang, Y., Park, S.Y., et al. (2018). Progressive fuzzy cation-π assembly of biological catecholamines. Sci. Adv. ***4***(9): eaat7457. https://doi.org/10.1126/sciadv.aat7457.
30. Waite, J.H., and Qin, X. (2001). Polyphosphoprotein from the adhesive pads of Mytilus edulis. Biochemistry ***40***(9): 2887–2893. https://doi.org/10.1021/bi002718x.
31. Silverman, H.G., and Roberto, F.F. (2007). Understanding marine mussel adhesion. Mar. Biotechnol. ***9***(6): 661–681. https://doi.org/10.1007/s10126-007-9053-x.
32. Zhao, H., and Waite, J.H. (2006). Linking adhesive and structural proteins in the attachment plaque of Mytilus californianus. J. Biol. Chem. ***281***(36): 26150–26158. https://doi.org/10.1074/jbc.M604357200.
33. Yu, J., Kan, Y., Rapp, M., et al. (2013). Adaptive hydrophobic and hydrophilic interactions of mussel foot proteins with organic thin films. Proc. Natl. Acad. Sci. USA ***110***(39): 15680–15685. https://doi.org/10.1073/pnas.1315015110.
34. Kang, S.M., Rho, J., Choi, I.S., et al. (2009). Norepinephrine: material-independent, multifunctional surface modification reagent. J. Am. Chem. Soc. ***131***(37): 13224–13225. https://doi.org/10.1021/ja905183k.
35. Waite, J.H. (2017). Mussel adhesion-essential footwork. J. Exp. Biol. ***220***(4): 517–530. https://doi.org/10.1242/jeb.134056.
36. Qiu, H., Qi, P., Liu, J., et al. (2019). Biomimetic engineering endothelium-like coating on cardiovascular stent through heparin and nitric oxide-generating compound synergistic modification strategy. Biomaterials ***207***(2019): 10–22. https://doi.org/10.1016/j.biomaterials.2019.03.033.
37. Yu, H., Yu, S., Qiu, H., et al. (2021). Nitric oxide-generating compound and bio-clickable peptide mimic for synergistically tailoring surface anti-thrombogenic and anti-microbial dual-functions. Bioact. Mater. ***6***(6): 1618–1627. https://doi.org/10.1016/j.bioactmat.2020.11.011.
38. Rafique, M., Wei, T., Sun, Q., et al. (2021). The effect of hypoxia-mimicking responses on improving the regeneration of artificial vascular grafts. Biomaterials ***271***(2021): 120746. https://doi.org/10.1016/j.biomaterials.2021.120746.
39. Huang, Z., Zhang, Y., Liu, R., et al. (2022). Cobalt loaded electrospun poly (ε-caprolactone) grafts promote antibacterial activity and vascular regeneration in a diabetic rat model. Biomaterials ***291***(2022): 121901. https://doi.org/10.1016/j.biomaterials.2022.121901.
40. Chen, X., Li, X., He, W., et al. (2023). Rational multivalency construction enables bactericidal effect amplification and dynamic biomaterial design. Innovation ***4***(5): 100483. https://doi.org/10.1016/j.xinn.2023.100483.
41. Lee, B.P., Messersmith, P.B., Israelachvili, J.N., et al. (2011). Mussel-inspired adhesives and coatings. Annu. Rev. Mater. Res. ***41***(2011): 99–132. https://doi.org/10.1146/annurev-matsci-062910-100429.
42. Kang, S.M., Park, S., Kim, D., et al. (2011). Simultaneous reduction and surface functionalization of graphene oxide by mussel-inspired chemistry. Adv. Funct. Mater. ***21***(1): 108–112. https://doi.org/10.1002/adfm.201001692.
43. Lee, H., Scherer, N.F., and Messersmith, P.B. (2006). Single-molecule mechanics of mussel adhesion. Proc. Natl. Acad. Sci. USA ***103***(35): 12999–13003. https://doi.org/10.1073/pnas.0605552103.
44. Li, W., Chan, C.-W., Li, Z., et al. (2023). All-perfluoropolymer, nonlinear stability-assisted monolithic surface combines topology-specific superwettability with ultradurability. Innovation ***4***(2): 100389. https://doi.org/10.1016/j.xinn.2023.100389.
45. Hong, S., Na, Y.S., Choi, S., et al. (2012). Non-covalent self-assembly and covalent polymerization co-contribute to polydopamine formation. Adv. Funct. Mater. ***22***(22): 4711–4717. https://doi.org/10.1002/adfm.201201156.
46. Wei, H., Ren, J., Han, B., et al. (2013). Stability of polydopamine and poly (DOPA) melanin-like films on the surface of polymer membranes under strongly acidic and alkaline conditions. Colloids Surf., B ***110***(2013): 22–28. https://doi.org/10.1016/j.colsurfb.2013.04.008.
47. Pillar-Little, E.A., Zhou, R., and Guzman, M.I. (2015). Heterogeneous oxidation of catechol. J. Phys. Chem. A ***119***(41): 10349–10359. https://doi.org/10.1021/acs.jpca.5b07914.
48. Zhang, C., Ou, Y., Lei, W.X., et al. (2016). $CuSO_4/H_2O_2$-induced rapid deposition of polydopamine coatings with high uniformity and enhanced stability. Angew. Chem. Int. Ed. ***55***(9): 3054–3057. https://doi.org/10.1002/anie.201510724.
49. Ma, Q., Shi, X., Tan, X., et al. (2021). Durable endothelium-mimicking coating for surface bioengineering cardiovascular stents. Bioact. Mater. ***6***(12): 4786–4800. https://doi.org/10.1016/j.bioactmat.2021.05.009.
50. Larsson, M., Rayzman, V., Nolte, M.W., et al. (2014). A factor XIIa inhibitory antibody provides thromboprotection in extracorporeal circulation without increasing bleeding risk. Sci. Transl. Med. ***6***(222): 222ra217. https://doi.org/10.1126/scitranslmed.3006804.
51. Shenoi, R.A., Kalathottukaren, M.T., Travers, R.J., et al. (2014). Affinity-based design of a synthetic universal reversal agent for heparin anticoagulants. Sci. Transl. Med. ***6***(260): 260ra150. https://doi.org/10.1126/scitranslmed.3009427.
52. Nih, L.R., Gojgini, S., Carmichael, S.T., et al. (2018). Dual-function injectable angiogenic biomaterial for the repair of brain tissue following stroke. Nat. Mater. ***17***(7): 642–651. https://doi.org/10.1038/s41563-018-0083-8.
53. Yang, Y., Qi, P., Ding, Y., et al. (2015). A biocompatible and functional adhesive amine-rich coating based on dopamine polymerization. J. Mater. Chem. B ***3***(1): 72–81. https://doi.org/10.1039/c4tb01236d.
54. Yang, Z., Yang, Y., Zhang, L., et al. (2018). Mussel-inspired catalytic selenocystamine-dopamine coatings for long-term generation of therapeutic gas on cardiovascular stents. Biomaterials ***178***(2018): 1–10. https://doi.org/10.1016/j.biomaterials.2018.06.008.
55. Yang, Z., Zhao, X., Hao, R., et al. (2020). Bioclickable and mussel adhesive peptide mimics for engineering vascular stent surfaces. Proc. Natl. Acad. Sci. USA ***117***(28): 16127–16137. https://doi.org/10.1073/pnas.2003732117.
56. Hu, Q., Fang, Z., Ge, J., et al. (2022). Nanotechnology for cardiovascular diseases. Innovation ***3***(2): 100214. https://doi.org/10.1016/j.xinn.2022.100214.
57. Goddard, J.M., and Hotchkiss, J. (2007). Polymer surface modification for the attachment of bioactive compounds. Prog. Polym. Sci. ***32***(7): 698–725. https://doi.org/10.1016/j.progpolymsci.2007.04.002.
58. Rusmini, F., Zhong, Z., and Feijen, J. (2007). Protein immobilization strategies for protein biochips. Biomacromolecules ***8***(6): 1775–1789. https://doi.org/10.1021/bm061197b.
59. Tiwari, V.K., Mishra, B.B., Mishra, K.B., et al. (2016). Cu-catalyzed click reaction in carbohydrate chemistry. Chem. Rev. ***116***(5): 3086–3240. https://doi.org/10.1021/acs.chemrev.5b00408.
60. Meng, X., and Edgar, K.J. (2016). "Click" reactions in polysaccharide modification. Prog. Polym. Sci. ***53***(2016): 52–85. https://doi.org/10.1016/j.progpolymsci.2015.07.006.
61. Scinto, S.L., Bilodeau, D.A., Hincapie, R., et al. (2021). Bioorthogonal chemistry. Nat. Rev. Methods Primers ***1***(1): 30. https://doi.org/10.1038/s43586-021-00028-z.
62. Meldal, M., and Tornøe, C.W. (2008). Cu-catalyzed azide-alkyne cycloaddition. Chem. Rev. ***108***(8): 2952–3015. https://doi.org/10.1021/cr0783479.
63. Knall, A.-C., and Slugovc, C. (2013). Inverse electron demand Diels-Alder (iEDDA)-initiated conjugation: a (high) potential click chemistry scheme. Chem. Soc. Rev. ***42***(12): 5131–5142. https://doi.org/10.1039/c3cs60049a.
64. Moses, J.E., and Moorhouse, A.D. (2007). The growing applications of click chemistry. Chem. Soc. Rev. ***36***(8): 1249–1262. https://doi.org/10.1039/b613014n.

65. DeForest, C.A., Polizzotti, B.D., and Anseth, K.S. (2009). Sequential click reactions for synthesizing and patterning three-dimensional cell microenvironments. Nat. Mater. ***8***(8): 659–664. https://doi.org/10.1038/nmat2473.
66. Reuther, J.F., Dees, J.L., Kolesnichenko, I.V., et al. (2017). Dynamic covalent chemistry enables formation of antimicrobial peptide quaternary assemblies in a completely abiotic manner. Nat. Chem. ***10***(1): 45–50. https://doi.org/10.1038/nchem.2847.
67. Schreiber, C.L., and Smith, B.D. (2019). Molecular conjugation using non-covalent click chemistry. Nat. Rev. Chem ***3***(6): 393–400. https://doi.org/10.1038/s41570-019-0095-1.
68. Wu, D., Sinha, N., Lee, J., et al. (2019). Polymers with controlled assembly and rigidity made with click-functional peptide bundles. Nature ***574***(7780): 658–662. https://doi.org/10.1038/s41586-019-1683-4.

ACKNOWLEDGMENTS

This work was supported by the National Natural Science Foundation of China (projects 82072072, 32171326, 82272157, 32261160372, and 82350710800), the Guangdong Basic and Applied Basic Research Foundation (2022B1515130010 and 2021A1515111035), the National Natural Science Foundation of China/Research Grants Council (NSFC/RGC) Joint Research Scheme (N_PolyU526/22), and the Leading Talent Project of Guangzhou Development District (2020-L013).

AUTHOR CONTRIBUTIONS

Z.D., H.W., and Z.Y. conceived and designed the experiments. Z.D. and F.Q. performed the experiments, analyzed the data, and prepared the figures. Z.D., H.W., and Z.Y. wrote the paper. X.M., L.T., W.Z., X.Z., N.H., and M.F.M. revised the paper. All authors discussed the results. Z.Y. and H.W. supervised the project.

DECLARATION OF INTERESTS

The authors declare no competing interests.

SUPPLEMENTAL INFORMATION

It can be found online at https://doi.org/10.1016/j.xinn.2024.100671.

LEAD CONTACT WEBSITE

https://yjsxt.smu.edu.cn/Open/TeacherInfo.aspx?id=KxpEVzhV5KMKbHx5UF750Q==